

TECHNOLOGY NEEDS FOR FOSSIL FUEL SUPERCRITICAL CO₂ POWER SYSTEMS

P. A. Strakey
Research Scientist
National Energy Technology Laboratory
Morgantown, WV
peter.strakey@netl.doe.gov

O. N. Dogan
Research Scientist
National Energy Technology Laboratory
Albany, OR
omer.dogan@netl.doe.gov

G. R. Holcomb
Materials Research Engineer
National Energy Technology Laboratory
Albany, OR
gordon.holcomb@netl.doe.gov

G. A. Richards
Focus Area Leader
National Energy Technology Laboratory
Morgantown, WV
geo.richards@netl.doe.gov

ABSTRACT

There has been an increase in interest over the past several years in supercritical CO₂ (sCO₂) cycles for power generation. For fossil energy applications, these cycles offer the potential for increased efficiency over Rankine cycles with inherent carbon capture using oxy-fuel combustion of natural gas or coal as the heat source. The increased efficiency is the result of the high density and low power of compression for CO₂ near the critical point as well as avoiding the latent heat of vaporization losses inherent in steam cycles. For oxy-fuel combustion strategies, carbon capture comes at virtually no additional expense as a high-pressure stream of CO₂ is the product of combustion, after water removal.

The application of sCO₂ cycles to commercial power generation does necessitate the development of new technologies in several areas including heat transfer, materials and combustion. This paper summarizes the current state of technology for sCO₂ power cycles and describes the various issues that still need to be addressed.

INTRODUCTION

Supercritical CO₂ (sCO₂) power cycles have been extensively studied for application with nuclear, solar, geothermal and other power sources, however there has been relatively little work on fossil fuel powered cycles, especially with CO₂ capture in mind. Some unique issues for fossil fuel systems are high-temperature combustion with carbon capture, high temperature recuperators, and materials compatibility. The real advantage over conventional Rankine cycles occurs for higher turbine inlet temperatures, typically in excess of 700°C, where steam cycles are limited by materials compatibility due primarily to high-temperature oxidation and creep. Thermal efficiency advantages are realized due to the lack of a latent heat of vaporization and subsequent boiler and condenser for a supercritical CO₂ working fluid. The high density of CO₂ above the critical point also allows for relatively low compression power compared to gas turbine fired Brayton cycles. There is also an inherent advantage of sCO₂ over steam cycles in terms

of a reduction in size of the turbomachinery, piping and valves due to the higher density of $s\text{CO}_2$ compared to steam, which translates into reduced capital costs.

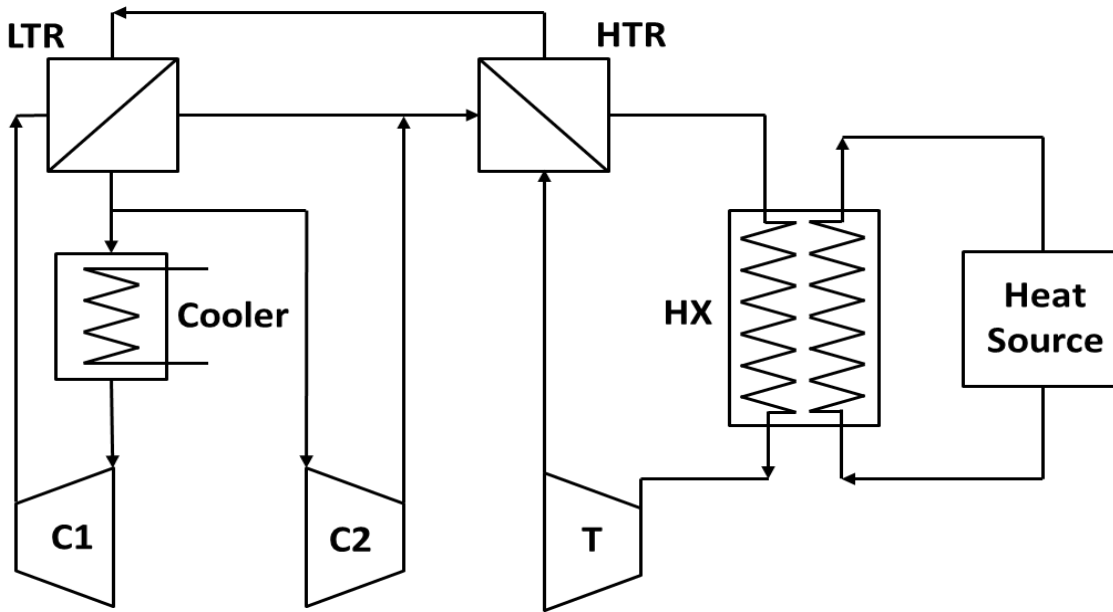


Figure 1: Recompression Brayton cycle with indirect heat source. LTR and HTR are low and high temperature recuperators, C1 and C2 are compressors, HX is a heat exchanger, and T is the turbine.

A number of variations of the simple $s\text{CO}_2$ Brayton cycle have emerged over the years, but for high temperature fossil fuel applications, the recompression cycle (Fig. 1) or the partial cooling cycle, which is similar to the recompression cycle with the addition of an additional compressor and cooler, were shown to provide the highest thermal efficiency, at least on paper [1,2]. The cycle shown in Figure 1 is for a closed or indirect fired system where the heat source is separated from the $s\text{CO}_2$ loop by a heat exchanger. The turbine inlet temperature of closed systems is limited by the maximum operating temperature of the combustor to working fluid heat exchanger ($\sim 700^\circ\text{C}$). Carbon capture for a closed system can be performed either pre- or post-combustion using oxy-fuel combustion or conventional air firing with a post combustion amine or membrane CO_2 separation system.

With recent advances in cryogenic oxygen production approaching 160 kWh/ton of O_2 , oxy-fired systems such as the NetPower cycle [3] are particularly attractive due to the inherent carbon capture nature of this cycle. In this approach, typically considered an open, or direct-fired system, natural gas or syngas fuel is combined with oxygen in a combustor and recycled CO_2 is used as a diluent to control the turbine inlet temperature. The maximum firing temperature of these systems is typically limited by metallurgical constraints of the high temperature recuperator to about 700°C with various film and convection cooling approaches used with the combustor and turbine components similar to what is done in Brayton cycles. With the relatively low pressure ratio at which these systems optimize ($\text{Pr}=3 \sim 10$), the turbine inlet temperature and pressure end up around 1100°C and 300 bar respectively. A simple, direct-fired Brayton cycle with oxy-fuel combustion and carbon sequestration is shown in Figure 2. In this cycle, there is no recompression loop as all of the flow leaving the low temperature recuperator is cooled to near ambient temperatures to remove the water from the system.

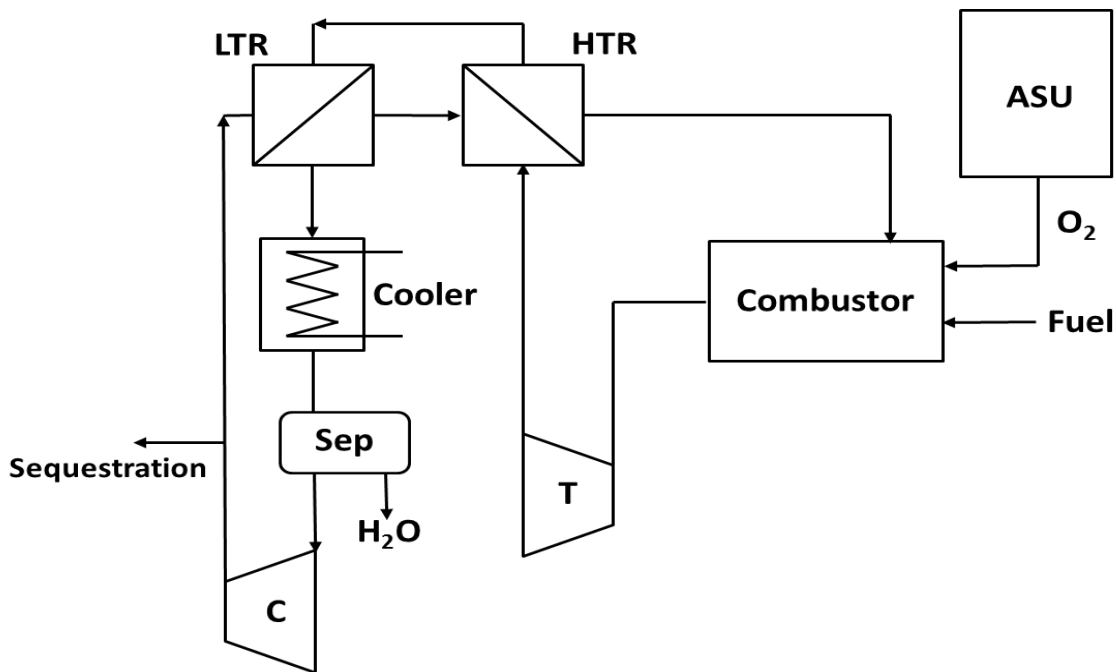


Figure 2: Direct fired simple sCO₂ Brayton cycle. LTR and HTR are low and high temperature recuperators, ASU is an air separation unit, Sep is the CO₂/H₂O separator, C is a compressor, and T is the turbine.

Recuperators

By nature, the sCO₂ cycle requires a large degree of heat recuperation with as much as half of the enthalpy entering the turbine coming from recuperation. The recuperator inlet temperatures can be in excess of 700°C and pressures as much as 300 bar for both direct and indirect fired systems. Conventional shell and tube heat exchangers are not practical due to the relatively low surface area to volume ratio ($< 100 \text{ m}^2/\text{m}^3$) which would dictate a massive and very expensive design. While there has been much progress recently with compact heat exchangers (typically $> 700 \text{ m}^2/\text{m}^3$), such as microchannel and printed circuit designs, there is still much work to be done to scale this technology in a cost effective manner to the gigawatt scale needed for commercial application. The largest issue is with the metallurgical and fabrication processes needed for operation with temperatures in excess of 700°C and pressures over 300 bar. Complex manifolding requirements for counter flow designs make this particularly challenging. Some specific issues for direct fired systems include corrosion due to the presence of water from the combustion products as well as fouling for coal fired systems. Coal fired systems are envisioned as an oxygen blown coal gasifier supplying syngas to the combustor with water quench and ash filtration steps between the gasifier and combustor to remove particulate material [3]. Even with good particulate removal there would still be various compounds in the exhaust gasses such as SO_x, NO_x and H₂O which could condense out to sulfuric and nitric acids and corrode and foul the recuperators. The capital cost as well as maintenance costs of the recuperators could prove to be a limiting factor in the realization of large scale commercial application.

Combustion

At pressures on the order of 300 bar, a direct fired sCO₂ combustor is more likely to resemble a rocket engine than any type of conventional gas turbine combustor. At these very high pressures and energy release densities, issues such as injector design, wall heat transfer and combustion dynamics may play a challenging role in combustor design. At these conditions, combustor design is an area where there is very little experience.

Also, since these pressures are well beyond current design experience, Computational Fluid Dynamics (CFD) modeling will not only be useful, but may be a necessity in the design process. As such, there is a need for chemical kinetic models valid at these conditions. Currently, most methane oxidation models are only validated at pressures below about 30 bar, an order of magnitude less than what is needed. CFD modeling to predict combustion dynamics or just overall mixing and performance requires validated chemical kinetic mechanisms for the governing reactions. Typically, for natural gas combustion, GRI-Mech¹ is used but this mechanism has only been developed and validated for pressures below about 10 bar which is more than an order of magnitude below the typical 300 bar of direct fired systems. Reduced mechanisms, as well as simple global reaction mechanisms are usually derived from the more detailed mechanisms like GRI-Mech and as such are only valid for combustion below about 10 bar. At higher pressures, 3-body recombination reactions deplete the radical pool as shown in the equilibrium calculation in Figure 3 which is for a stoichiometric CH₄/O₂/CO₂ mixture with a nominal temperature of about 2000K. Also note the increase in temperature as pressure is increased due to the decrease in radical concentrations and subsequent increase in product gas formation (CO₂ and H₂O).

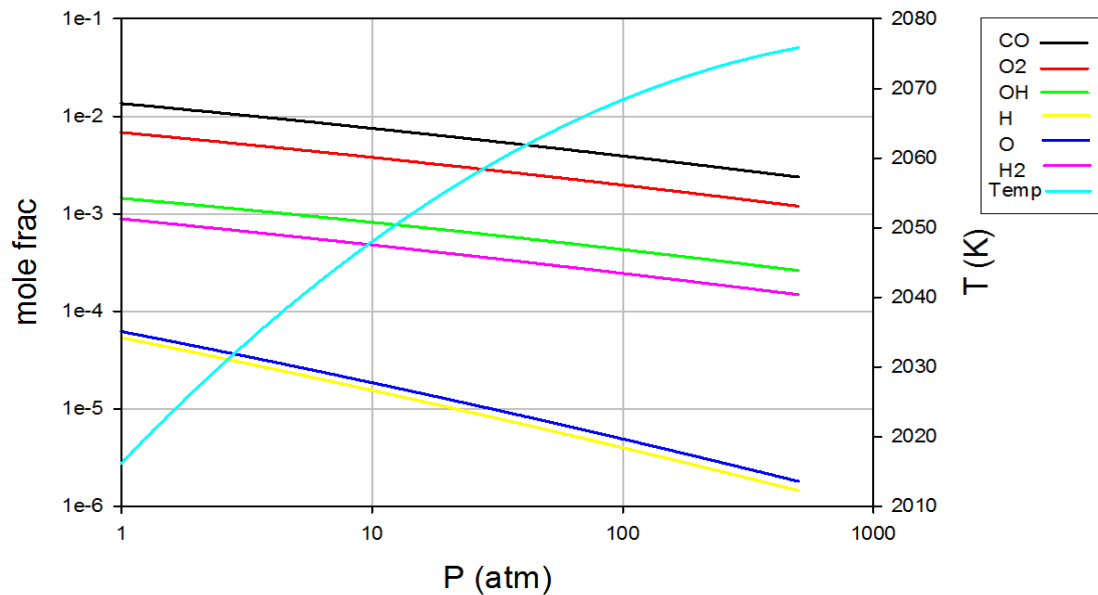


Figure 3: Equilibrium calculation for stoichiometric methane-oxygen mixture with carbon dioxide diluent.

The extrapolation of low pressure kinetic mechanisms to the very high pressures of sCO₂ cycles introduces a large uncertainty in reaction rates and heat release. Confidence in CFD and other modeling predictions require validation of candidate mechanisms using shock tube, combustion bomb and flame

¹ GRI-MECH 3.0, http://www.me.berkeley.edu/gri_mech/, accessed 8/7/2014.

speed measurements at high pressure. For coal based systems operating on coal syngas, even more data is needed for the prediction of high pressure syngas chemistry with potential contaminants.

For oxy-fired combustion, NO_x formation is not really an issue so the preferred combustion approach is diffusion flame combustion where the fuel and oxidizer are mixed and burnt in the combustion chamber. It is well known in the gas turbine community that diffusion flame combustors are inherently more resistant to combustion dynamics than premixed combustors. However, it is also well known that rocket engine combustors, which are all diffusion based, have a long history of combustion dynamics problems due to the very large pressure and large energy release density which tends to couple with the resonant acoustic modes of the combustion chamber. Problems with combustion dynamics are typically discovered and solved with full scale hardware testing through the use of Helmholtz resonators, baffles and injector design modifications. Some of the most damaging coupling occurs in the 1-10 kHz range due to combustor tangential and radial acoustic modes and is known as screech in the rocket engine community. Recently, some promise has been shown with CFD modeling using compressible Large Eddy Simulations (LES) to predict combustion dynamics, though this is computationally expensive and far from maturity.

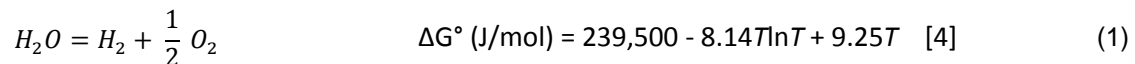
Issues for structural materials

Materials selection for components (turbines, heat exchangers) exposed to a specific sCO₂ cycle is challenging since materials have not been tested commonly under these conditions. However, materials selected for advanced ultra-supercritical (A-USC) steam systems are a good starting point for sCO₂ cycles. Required key properties of materials employed in fossil fuel sCO₂ cycles will depend on the application temperature, pressure and environment. It is expected that these systems will use sCO₂ as working fluid at temperatures up to 800°C and pressures up to 350 bar. Heat exchangers will be employed to utilize the heat from oxyfuel combustion. Therefore, the heat exchanger materials will be exposed to dual environments (sCO₂ and oxyfuel combustion gases) making them increasingly vulnerable to high-temperature corrosion. Below, high-temperature oxidation behavior of structural materials in steam and sCO₂ is compared.

High-temperature oxidation

Equilibrium oxygen partial pressure in steam and CO₂

Assuming that alloy and oxide surfaces are similarly catalytic for the following equilibrium dissociation reactions of water and CO₂,



oxidizing potentials of steam and CO₂ are similar especially at higher temperatures as shown in Fig 4a. Furthermore, the difference between the oxygen partial pressures from the two dissociation reactions becomes negligible when they are compared to the equilibrium oxygen partial pressures required for the formation of relevant metal oxides which are much lower than those provided by the dissociation reactions of water and CO₂ (Fig 4b).

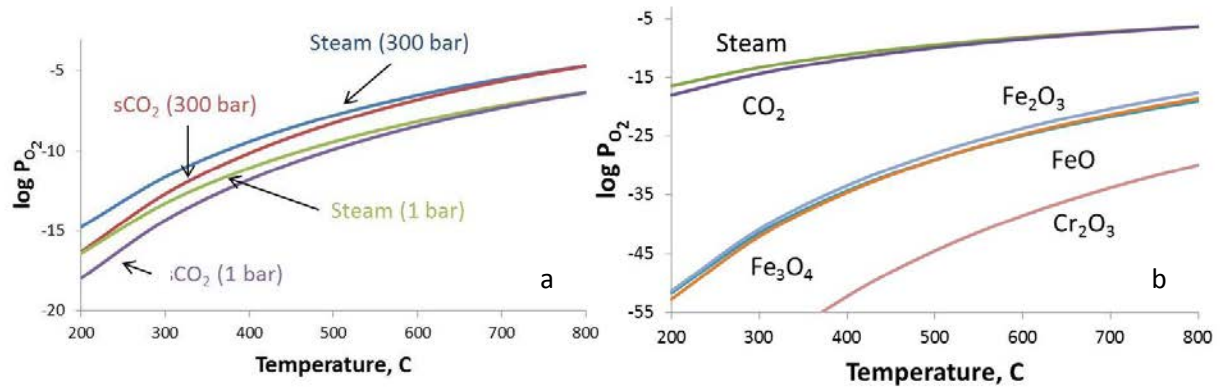


Figure 4: Oxygen partial pressures from dissociation of H_2O and CO_2 at 1 and 300 bar as a function of temperature (a) and the same data compared to the oxygen partial pressures required to form iron and chromium oxides at 1 bar (b).

Kinetics of oxidation in sCO_2 on power plant alloys

There is very limited data for oxidation kinetics of ferritic/martensitic steels in sCO_2 [5, 6]. Relatively short time exposures of 9Cr steels to sCO_2 showed similar kinetics of oxidation to that in steam as shown in Figure 5. The line representing the parabolic rate constant ($k_p = \Delta W^2/2t$, where ΔW is mass gain and t is time of exposure) for oxidation in steam is an average of the numerous data for T91 steel, at all pressures, as compiled in reference [7]. High pressure data for T91 are also plotted in the figure [8, 9]. It is important to note that the sCO_2 data is for relatively short term exposures (310 and 500 hours) compared to the data for steam.

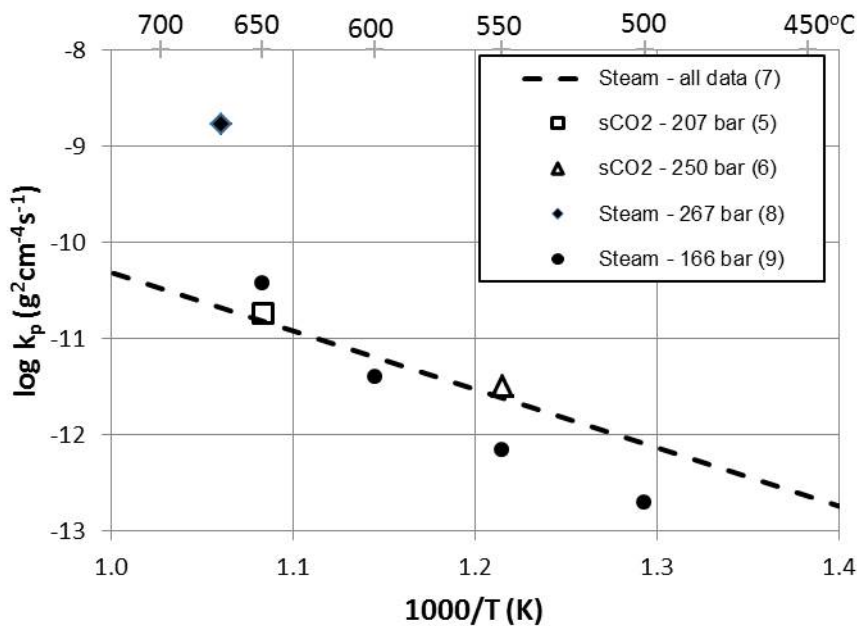


Figure 5: Parabolic rate constant for oxidation of T91 steel in sCO_2 compared to that in steam.

There is mass gain data in sCO₂ up to 3000 hours for several austenitic steels as shown in Fig 6 [10, 11]. In this figure, the parabolic rate constants calculated from the mass gain during the sCO₂ exposures are compared to the average parabolic rate constants for coarse-grained 300 series at all pressures and PMCr at 17 bar for steam exposures compiled in reference [7]. In steam, as the pressure increases, fine-grain 300 series steels oxidize faster and behave more like coarse-grain alloys [7,8]. 316 stainless steel demonstrates the fastest oxidation kinetics in sCO₂ at 650°C and 200 bar. Higher Cr steels (310, AL-6XN, and 800H) exhibit much less mass gain in sCO₂ at 650°C and 200 bar compared to 316 steel under the same conditions. At 550°C and 250 bar of CO₂, the oxidation behavior of 316 steel is similar to that of the 800H alloy. Unfortunately, there is no grain size data available for the steels exposed to sCO₂. All the kinetic data available for oxidation in sCO₂ fall between the best fit lines representing the parabolic rate constants of the fine-grained (PMCr) and the coarse-grained austenitic steels oxidized in steam.

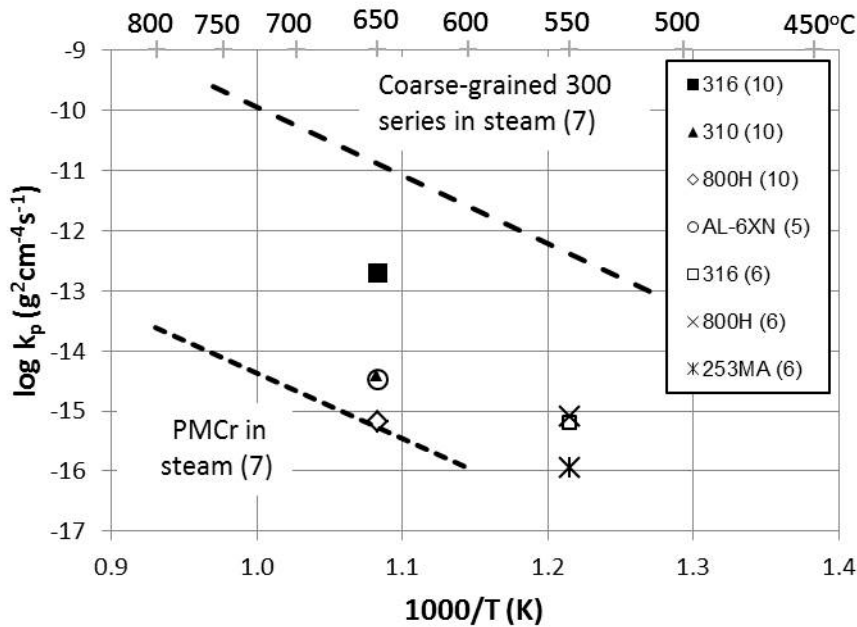


Figure 6: Parabolic rate constant of austenitic steels in sCO₂ and steam. The PMCr (17 bar) line can be viewed as the lower limit for the grain size effect (fine-grained) where there is infinite supply of Cr to the alloy-scale interface.

Available data on oxidation kinetics of Ni-based alloys in general show that they gain much less mass in sCO₂ compared to steam at 650°C. Figure 7 illustrates this point by plotting the mass gain from the high-pressure oxidation data in reference [8] for IN617, H230, IN740, H263, and H282 in steam and the data reported in reference [11] for PE-16, H230, and Alloy 625 in sCO₂. In steam at lower pressures, Ni-base alloys show behavior close to that of the PMCr line [7,8].

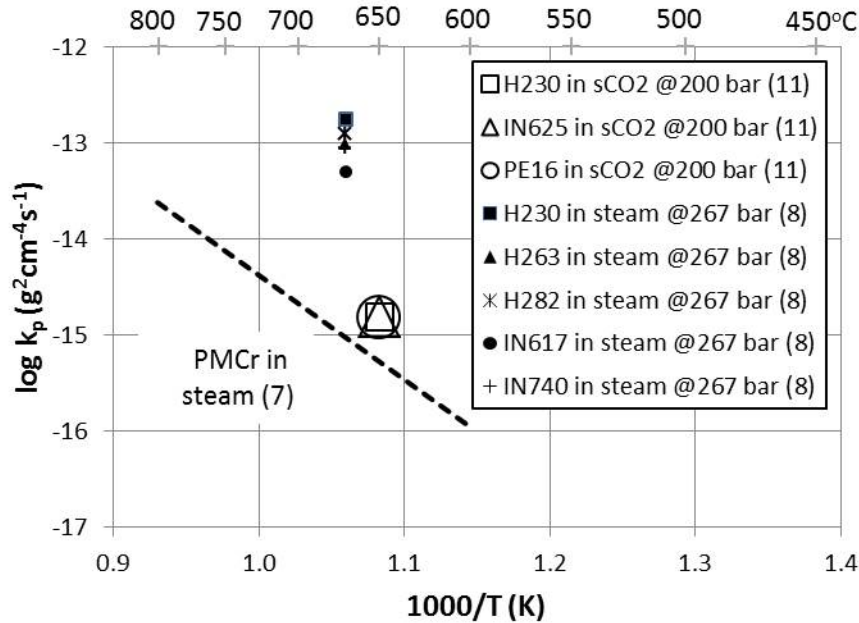


Figure 7: Parabolic rate constants for Ni-based alloys in high pressure steam and CO₂.

Characterization of oxidation products

Exposure of ferritic/martensitic 9 Cr steels to steam at high temperatures results in formation of a layered oxidation structure as illustrated schematically in Figure 8. First, an external magnetite scale on the surface forms and it grows through diffusion of Fe cations from the metal to the scale-gas interface. At the same time, a layer of spinel forms via inward diffusion of oxygen anions through the magnetite (Fe₃O₄) scale to the scale-metal interface. The spinel layer develops into a Fe-rich spinel layer at the original metal surface and a Cr-rich spinel below it. The spinel oxidation zone can evolve into multiple layers of spinel of different compositions. Porosity also develops in the magnetite layer and at the interface between magnetite and spinel. The pores can facilitate spallation of the magnetite scale in cyclic operations. After extended exposure, reduction in Fe-cation flux to the magnetite-steam surface may result in the formation of hematite (Fe₂O₃) instead of magnetite. The hematite can be either as discrete areas or a continuous layer. Limited short term exposures of 9 Cr steels to sCO₂ show an oxidation structure very similar to that obtained in high-temperature oxidation in steam [5, 8]. The primary difference in the oxidation structure is the lack of hematite on the 9 Cr steel exposed to sCO₂ likely because of the much shorter exposure times used in sCO₂ compared to the steam exposures.

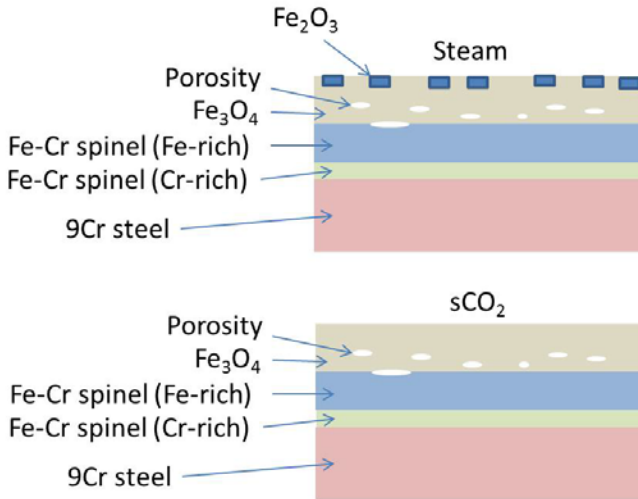


Figure 8: Schematic illustration of formation of oxidation products on 9 Cr steels in steam and sCO₂.

Figure 9 shows that oxidation products on the lower Cr austenitic steels exposed to steam at high temperatures are similar to those on the 9Cr steels discussed above. The primary external scale is magnetite with hematite islands forming at extended exposures. Pores also develop within magnetite. The spinel layer composition includes Ni and Mn in addition to Fe and Cr. Higher Cr austenitic steels exhibit the same oxidation layers plus a thin Cr₂O₃ layer between the spinel and the metal after exposure to steam.

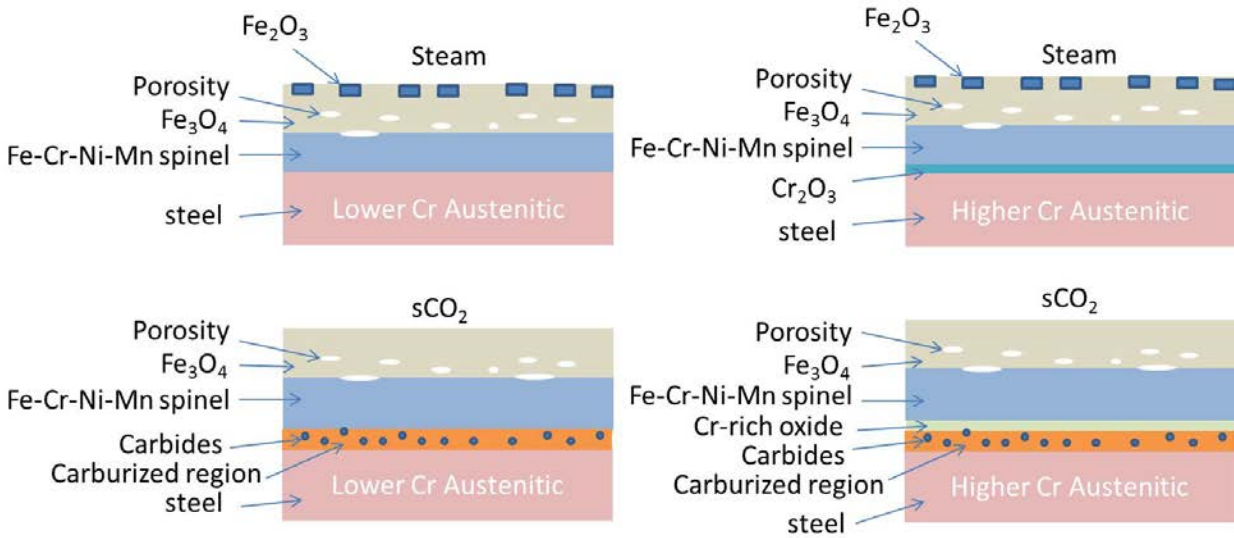


Figure 9: Schematic illustration of formation of oxidation products on austenitic steels in steam and sCO₂.

Exposing the austenitic steels to $s\text{CO}_2$ at temperatures similar to steam exposure results in similar oxidation structures to those presented above with one exception [10]. A carburized layer forms below the oxide layers. Depending on the composition of the steel, this layer may contain carbide particles.

Typically a Ni-Cr-Mn spinel is observed on Ni-based alloys exposed to steam at high temperatures (Figure 10). Sometimes, Cr_2O_3 mixed in with spinel is also observed. Often times this protective oxide layer contains porosity. Below this external scale, an internal oxidation zone contains oxide particles of alloying elements such as Al_2O_3 . Sometimes, oxidation products penetrate deeper into the alloy via grain boundary oxidation. Relatively short term exposures (3000 hours) of Ni-based alloys to $s\text{CO}_2$ at 650°C and 200 bar showed an external scale (spinel + chromia + porosity) that is similar to that observed in steam exposures [11]. However, no internal oxidation has been observed in these alloys exposed to $s\text{CO}_2$ [11]. The lack of internal oxidation may be due to the shorter duration of exposure (longer exposures may result in internal oxidation) or protective external scale which doesn't allow sufficient oxygen ion diffusion to the metal – scale interface.

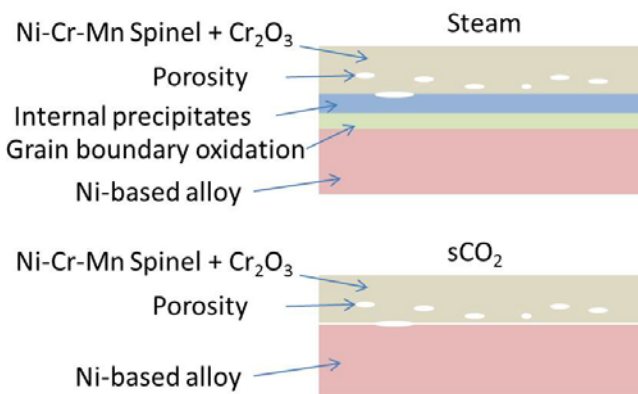


Figure 10: Schematic illustration of formation of oxidation products on Ni-based alloys in steam and $s\text{CO}_2$.

An in-depth investigation of carburization was reported on 9Cr-1Mo ferritic steel [12]. Carburization of 9Cr-1Mo steel increases with pressure from 1 bar to 250 bars in CO_2 at 550°C . Increasing pressure increases the deposition of carbon in the inner spinel scale. The free carbon on the alloy surface can reach the scale-alloy interface via cracks and grain boundaries in the scale and either dissolve or form carbides in alloys, thus changing the properties of the alloy and likely lowering the useful life of component. Carburization data in the $s\text{CO}_2$ cycles is also very limited. Carburization potential can be modeled thermodynamically as a function of environment and temperature. Quadakkers et al [13] demonstrated such modeling for corrosion in primary circuit helium of high temperature gas cooled reactors containing CO and other gas impurities.

Low cycle fatigue and creep-fatigue

It was shown that low cycle fatigue (LCF) and creep-fatigue life of metallic materials can be reduced due to high-temperature oxidation [14-19]. The effect is dependent on the operation or test conditions. Intergranular crack initiation can be facilitated if the grain boundaries near the stress concentration are oxidized. The effect of oxidation in the crack propagation stage is also observed. Oxidation-assisted intergranular crack growth occurs if the cyclic oxidation damage is greater than the fatigue damage.

Given that $s\text{CO}_2$ is an effective oxidizer as discussed above, it is expected that exposure of power plant materials to the $s\text{CO}_2$ conditions will influence their LCF and creep-fatigue life. However, there are no reports of investigation of this subject in the open literature.

CONCLUSIONS

There has been an increase in interest over the past several years in supercritical CO_2 ($s\text{CO}_2$) cycles for power generation. For fossil energy applications, these cycles offer the potential for increased efficiency over Rankine cycles with inherent carbon capture using oxy-fuel combustion of natural gas or coal as the heat source. The increased efficiency is the result of the high density and low power of compression for CO_2 near the critical point as well as avoiding the latent heat of vaporization losses inherent in steam cycles. For oxy-fuel combustion strategies, carbon capture comes at virtually no additional expense as a high-pressure stream of CO_2 is the product of combustion, after water removal.

Some specific areas where technology development is needed include; high-pressure chemical kinetic mechanisms for natural gas and syngas combustion, high-pressure combustor development for open cycles, high temperature and pressure recuperators, and materials suitable for the specific conditions of $s\text{CO}_2$ cycles.

A review of the available materials literature revealed a comparison of oxidation behaviors (kinetics and scale morphologies) of alloys in high pressure steam and $s\text{CO}_2$ and found many similarities. The materials solutions that are used in high pressure steam show promise for use in $s\text{CO}_2$, with the caveat that the $s\text{CO}_2$ exposures were relatively short in duration:

- Ferritic/martensitic 9 Cr steels had similar kinetics and scale morphologies in high pressure steam and $s\text{CO}_2$.
- Austenitic steels have oxidation behavior that can be highly dependent upon grain size. In steam, as the pressure increases the oxidation behavior of fine-grain steels increases and behave more like coarse-grain materials. In $s\text{CO}_2$, the cited references do not report grain size, but the oxidation kinetics lie between that of fine-grain steels (at low pressure) and coarse-grain steels. A carburization layer was reported for austenitic steels in $s\text{CO}_2$.
- Ni-base alloys exhibited less oxidation in $s\text{CO}_2$ than in high pressure steel (in this case the steam exposures were also of short duration). Similar scale morphologies were reported.

While the challenges remain significant and require a focused research effort, there don't appear to be any show stopping problems to commercialization of this technology.

REFERENCES

1. Martin, K. and Vaclav, D., *Thermodynamic Analysis and Comparison of Supercritical Carbon Dioxide Cycles*. Supercritical CO_2 Power Cycle Symposium, May 24-25, 2011, Boulder, CO.
2. Angelo, G., *Carbon Dioxide Condensation Cycles for Power Generation*. J. Eng. Gas Turbines and Power, July, 1968, pp. 287-295.
3. Allam, R. J., et. al., *High Efficiency and Low Cost of Electricity Generation From Fossil Fuels While Eliminating Atmospheric Emissions, Including Carbon Dioxide*. Energy Pcedia, **37**, 2013, pp. 1135-1149.
4. Gaskell, D.R., *Introduction to Metallurgical Thermodynamics*. 2 ed. 1981: McGraw-Hill Book Company.

5. Tan, L., et al., *Corrosion of austenitic and ferritic-martensitic steels exposed to supercritical carbon dioxide*. Corrosion Science, 2011. **53**(10): p. 3273-3280.
6. Rouillard, F., F. Charton, and G. Moine. *Corrosion behaviour of different metallic materials in supercritical CO₂ at 550C and 250 bars*. in *SCCO₂ Power Cycle Symposium*. 2009. Troy, NY.
7. Wright, I.G. and R.B. Dooley, *A review of the oxidation behaviour of structural alloys in steam*. International Materials Reviews, 2010. **55**(3): p. 129-167.
8. Holcomb, G.R., *High Pressure Steam Oxidation of Alloys for Advanced Ultra-supercritical Conditions*. Oxidation of Metals, 2014.
9. Angell, M.G., S.K. Lister, and A. Rudge, *The effect of steam pressure on oxidation behavior of annealed 9Cr 1Mo boiler tubing materials*, in *15th International Conference on Properties of Water and Steam*. 2008, VDI-Gesellschaft Energietechnik: Dusseldorf.
10. Cao, G., et al., *Corrosion of austenitic alloys in high temperature supercritical carbon dioxide*. Corrosion Science, 2012. **60**: p. 246-255.
11. Firouzdar, V., et al., *Corrosion of a stainless steel and nickel-based alloys in high temperature supercritical carbon dioxide environment*. Corrosion Science, 2013. **69**: p. 281-291.
12. Rouillard, F., et al., *Corrosion of 9Cr Steel in CO₂ at Intermediate Temperature II: Mechanism of Carburization*. Oxidation of Metals, 2012. **77**(1-2): p. 57-70.
13. Quadackers, W.J. and H. Schuster, *Corrosion of High-Temperature Alloys in the Primary Circuit Helium of High-Temperature Gas-Cooled Reactors .1. Theoretical Background*. Werkstoffe Und Korrosion-Materials and Corrosion, 1985. **36**(4): p. 141-150.
14. Chen, X., et al., *Effect of creep and oxidation on reduced fatigue life of Ni-based alloy 617 at 850 degrees C*. Journal of Nuclear Materials, 2014. **444**(1-3): p. 393-403.
15. Evans, A.G., et al., *A mechanism governing oxidation-assisted low-cycle fatigue of superalloys*. Acta Materialia, 2009. **57**(10): p. 2969-2983.
16. He, M.Y. and A.G. Evans, *A model for oxidation-assisted low cycle fatigue of superalloys*. Acta Materialia, 2010. **58**(2): p. 583-591.
17. Prakash, D.G.L., et al., *Crack growth micro-mechanisms in the IN718 alloy under the combined influence of fatigue, creep and oxidation*. International Journal of Fatigue, 2009. **31**(11-12): p. 1966-1977.
18. Tong, J., et al., *Creep, fatigue and oxidation in crack growth in advanced nickel base superalloys*. International Journal of Fatigue, 2001. **23**(10): p. 897-902.
19. Totemeier, T.C. and H.B. Tian, *Creep-fatigue-environment interactions in INCONEL 617*. Materials Science and Engineering a-Structural Materials Properties Microstructure and Processing, 2007. **468**: p. 81-87.